

Article

Influence of the Presence of a Nano-Sized Filler in the Generation of Microplastics from Polypropylene Nanocomposites

Marco Morreale ^{1,*} , Erika Indovino ² , Luigi Botta ^{2,3}  and Francesco Paolo La Mantia ^{2,3,*} 

¹ Department of Engineering and Architecture, Kore University of Enna, Cittadella Universitaria, 94100 Enna, Italy

² Department of Engineering, University of Palermo, Viale delle Scienze, 90128 Palermo, Italy; erika.indovino@unipa.it (E.I.); luigi.botta@unipa.it (L.B.)

³ National Interuniversity Consortium of Materials Science and Technology (INSTM), Via Giusti 9, 50121 Florence, Italy

* Correspondence: marco.morreale@unikore.it (M.M.); francescopaolo.lamantia@unipa.it (F.P.L.M.)

Abstract

The widespread and exponentially increasing use of polymer-based commodities is, nowadays, a basically intrinsic element of contemporary life as well as a substantial environmental concern. Moreover, it has led to significant adverse consequences especially when recovery and recycling are unsatisfactory, conditions favoring the formation of microplastics and nanoplastics with significant consequences on aquatic systems, soil, atmosphere, as well as biota and human health. Although the topic is undergoing massive investigation and research, there is less data about the behavior of multiphase polymer systems, especially as far as nanocomposites are concerned. In this paper, we simulated the two main generation mechanisms of micro- and nanoplastics (photo-oxidation and mechanical fragmentation) of a polypropylene/clay nanocomposite and systematically characterized the amount and size distribution of the obtained microplastics. It was found that the presence of this nanoclay can lead to reduced microplastic generation, due to mitigation of the photo-oxidation processes.

Keywords: polymer nanocomposites; microplastics; polypropylene

1. Introduction

The massive utilization of plastics and polymer-based commodities constitutes both an intrinsic element of contemporary life and a substantial environmental concern. The exponential increase in the production and consumption of such materials has led to significant adverse consequences, especially in contexts where recovery and recycling operations are unsatisfactory. Under these conditions, the formation of microplastics, mesoplastics, and nanoplastics is practically inevitable [1–18], with significant consequences affecting the aquatic systems, soils, and the atmosphere, as well as biota and human health [19–21].

Microplastics and nanoplastics are usually defined as polymer particulate matter showing dimensions below 5 mm. Their environmental occurrence derives mainly from two separate sources: intentional introduction (primary microplastics) and inadvertent generation (secondary microplastics). Primary microplastics are, for instance, particles deliberately engineered with dimensions less than 5 mm, such as those incorporated in



Academic Editor: Joanna Ryzd,
Marta Musioł and Barbara
Zawidlak-Węgrzyńska

Received: 5 December 2025

Revised: 29 January 2026

Accepted: 29 January 2026

Published: 3 February 2026

Copyright: © 2026 by the authors.

Licensee MDPI, Basel, Switzerland.

This article is an open access article distributed under the terms and conditions of the [Creative Commons Attribution \(CC BY\) license](https://creativecommons.org/licenses/by/4.0/).

certain cosmetic formulations, paints, pharmaceuticals, pellets, and textile fibers [18,22,23]. Secondary microplastics, by contrast, originate from the degradation and fragmentation of larger polymeric items, thereby yielding micro- and submicrometric particles [24–26].

A critical review of the literature reveals numerous investigations [18,23,27–34] concerning the generation of microplastics and their environmental impacts, predominantly addressing conventional polymers such as polyethylene [31,32] and polypropylene [33]. There is even less information about the behavior of multiphase systems, such as polymer blends, which may be microplastic generators [35]. In a previous paper [36], we examined the influence of morphology and compatibilization of an uncompatibilized and compatibilized polypropylene/poly(ethylene terephthalate) (PP/PET) blend by simulating, in a very simple and straightforward way, the fragmentation induced by both the mechanical stress and the photo-oxidation, and by conducting a comprehensive characterization of the size distribution of the obtained microplastics. Our results demonstrated that photo-oxidized samples exhibited a markedly enhanced propensity for micro- and nanoplastic generation. Importantly, compatibilization substantially mitigated such release, an effect ascribed to improved interfacial adhesion between the two phases (i.e., polymer matrix and dispersed polymer particles).

However, to date, limited information is available about the issue of microplastic generation in relationship to polymer nanocomposites. To the best of our knowledge, only a few studies [37–40] are available, and in most cases they focus more on collection and measurement procedures, rather than systematic assessment of differential release from neat polymers and their nanocomposites.

Alipour et al. [37], for instance, developed an exposure chamber and a procedure for the collection and analysis of the released particles, in order to obtain qualitative data on the release during the degradation, without mechanical stresses, of a clay-filled polypropylene (PP) nanocomposite. They observed that clay platelets, especially when exfoliated and close to the surface, could leave the polymer matrix without abrasive or mechanical forces.

Bossa et al. [38] also developed a new protocol, in this case regarding abrasion of multi-walled carbon nanotubes (MWCNTs)–poly(ethylene terephthalate glycol) (PETG) nanocomposites. They highlighted that the risk of exposure to MWCNTs detaching from the nanocomposites seems to be low but requires further investigation, since they also observed that the abrasion and release was likely dependent on the matrix and therefore may differ significantly as far as other polymer matrices are concerned.

Sahle-Demessie et al. [39] investigated the mechanisms behind the accelerated weathering of epoxy–MWCNT nanocomposites, finding that the main factors affecting the degradation were the matrix and the ultraviolet irradiation dose; they focused especially on the chemical and toxicity characterization of the released material.

Sipe et al. [40] applied a novel apparatus and protocol to quantify abrasion of silver nanoparticles (AgNP)–PETG composites under various power inputs over time. They found, in agreement with other studies, that the polymer matrix, rather than the nanofillers, is more likely to critically determine the abrasion rate.

However, as is predictable from this brief analysis, there is little data about the characterization of both mass and size distribution of the microplastics released under the combined mechanical and photo-oxidative stress of polymer nanocomposites.

In this paper, therefore, we aim to address this gap by simulating the fragmentation induced by both mechanical stress and photo-oxidation on a PP–clay nanocomposite, and by conducting a characterization of the amount and size distribution of the obtained microplastics.

2. Materials and Methods

The materials utilized in this work were a PP extrusion grade commercialized by LiondellBasell (Ferrara, Italy) as “Moplen[®] RP340H”, having a melt flow rate (MFR) equal to 1.8 g/10 min (at 230 °C and 2.16 kg); and an organically modified clay sample, marketed as Dellite[®] 72T (Laviosa Mineraria, Livorno, Italy), and known to derive from a naturally occurring montmorillonite, specially purified and modified with a stoichiometric content of quaternary ammonium salt (dimethyl dihydrogenated tallow ammonium).

The nanocomposites containing 5 wt% clay were prepared by melt compounding, using a Brabender (Duisburg, Germany) PLE330 internal mixer operating at a 190 °C temperature, 60 rpm rotating speed, 5 min processing duration.

The sheets (approx. 400 µm thick) for the subsequent tests were prepared by compression molding using a Carver (Wabash, IN, USA) laboratory press operating at 190 °C, pressure 300 psi, for 3 min.

Photo-oxidation was simulated by means of Q-UV (Q-Labs Corp., Westlake, OH, USA) accelerated weathering equipment, using eight UVB-313 lamps (ASTM G53-96) with a cycle consisting of 8 h exposure to UV rays at 70 °C and 4 h of water condensation at 50 °C, up to a maximum of 192 h.

Mechanical characterization was performed through tensile tests on neat (i.e., not photo-oxidized) and photo-oxidized samples (at least five for each sample type), by means of an Instron (Norwood, MA, USA) mod. 3365 universal testing machine. Deformation speed was set at 1 mm/min up to the first mm of actual deformation, and then 100 mm/min up to specimen breaking. The measured tensile properties, i.e., elastic modulus (E), tensile strength (TS), and elongation at break (EB), were therefore obtained, and the dimensionless values as a function of the photo-oxidation time (i.e., average value at time “t” divided by the average value at time = 0) were also calculated.

Microplastics generated from the samples were laboratory-produced using the procedure already described in previous papers [36,41]. In more detail, all the samples (photo-oxidized, or not) were ground by means of a Fritsch (Idar-Oberstein, Germany) blade mill operating at 2800 rpm for 10 s. The fragments were accurately recovered and weighed and then sieved using a series of inox steel sieves with mesh ranging from 5 mm to 500 µm (5 mm/2 mm/1 mm/500 µm), and every separated fragment was finally weighed, all weight measurements being performed on triplicates using a Kern (Balingen, Germany) analytical balance. Variability of measurements was below detection.

Spectroscopic analysis on the photo-oxidized samples was carried out using a Perkin-Elmer (Norwalk, CT, USA) FT-IR/ATR SpectrumOne spectrometer and the related Spectrum One software. The spectra (average of 16 scans) were collected in the range 4000–450 cm⁻¹, with an optical resolution of 4 cm⁻¹.

Interlayer distances were measured by X-ray diffraction (XRD) tests at room temperature by means of a PANalytical (Almelo, The Netherlands) Empyrean diffractometer system, equipped with a Cu X-ray source (operating at 40 KV and 30 mA, with an incident X-ray wavelength $\lambda = 1.5418 \text{ \AA}$). The interlayer distance was calculated using the well-known Bragg’s law.

Thermogravimetric analysis (TGA) was carried out using a Netzsch (Selb, Germany) STA 449 F1 Jupiter thermogravimetric analyzer; the samples were heated from 20 °C to 700 °C with a heating rate of 10 °C min⁻¹ in air.

The investigated samples are, for the sake of clarity, summarized with their codes in the following Table 1.

Table 1. Investigated samples and their codes.

| Sample | Sample Code |
|---|-------------|
| Polypropylene, 0 h photo-ox. | PP, PP_0hr |
| Polypropylene, 48 h photo-ox. | PP_48hr |
| Polypropylene, 96 h photo-ox. | PP_96hr |
| Polypropylene, 192 h photo-ox. | PP_192hr |
| Polypropylene/clay nanocomposite, 0 h photo-ox. | NPP_0hr |
| Polypropylene/clay nanocomposite, 48 h photo-ox. | NPP_48hr |
| Polypropylene/clay nanocomposite, 96 h photo-ox. | NPP_96hr |
| Polypropylene/clay nanocomposite, 192 h photo-ox. | NPP_192hr |

3. Results and Discussion

Figure 1 reports the average values (and the deviation bars) of the main mechanical properties, for neat (0 h) and photo-oxidized (48 h, 96 h) PP and NPP samples. The 192 h samples were so brittle that it was impossible to perform the mechanical characterization.

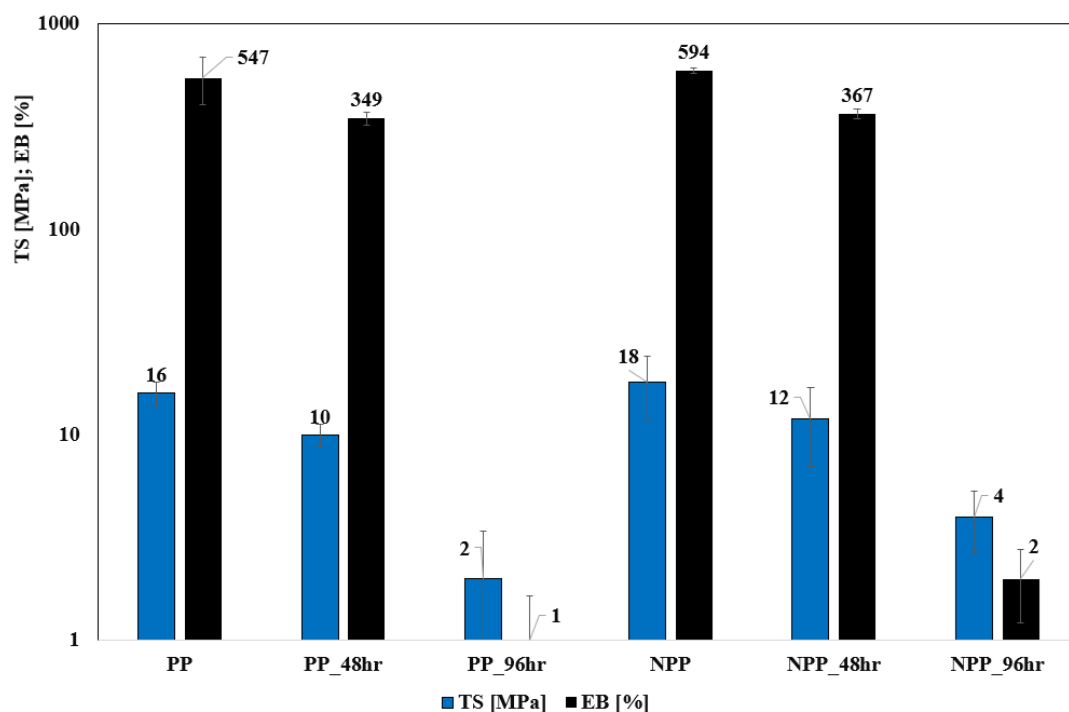


Figure 1. Average values (and the standard deviations) of the main mechanical properties for neat (0 h) and photo-oxidized (48 h, 96 h) PP and NPP samples.

As expected, NPP shows higher values of the tensile properties, and the enhancement of TS and EB suggests that the nanoclay filler is likely to be intercalated according to previous findings on similar systems [42]. In order to find confirmation for this statement, XRD analysis was performed and the main results are shown in Table 2 (diffractograms reported in the Supplementary Materials, see Figure S1). It can be observed that the interlayer distance of the nanoclay moderately increases in the NPP sample, proving that a certain degree of intercalation actually occurs and thus confirming the explanation previously proposed.

Table 2. Main XRD peak and interlayer distance for pristine Dellite and NPP.

| Sample | Main Peak, 2θ [°] | Interlayer Distance, d_{001} [nm] |
|---------|--------------------------|-------------------------------------|
| Dellite | 3.36 | 2.62 |
| NPP | 3.08 | 2.86 |

Regarding the photo-oxidized samples, there is an obvious worsening of all the properties; however, it can be clearly observed that the decrease is, on a relative basis, higher in the PP samples when compared to the NPP ones. This can be better evaluated by considering the dimensionless data reported in Table 3 as a function of the photo-oxidation time.

Table 3. Dimensionless values as a function of the photo-oxidation time.

| Sample | TS | EB |
|-----------|------|--------|
| PP, 0 h | 1 | 1 |
| PP, 48 h | 0.62 | 0.64 |
| PP, 96 h | 0.13 | 0.0018 |
| NPP, 0 h | 1 | 1 |
| NPP, 48 h | 0.67 | 0.62 |
| NPP, 96 h | 0.22 | 0.0035 |

The dimensionless data reported clearly demonstrate that the NPP samples undergo less severe effects due to photo-oxidation, resulting in a lower decrease in the mechanical properties. This indicates that the nanofiller contributes to mitigating the embrittlement related to the photo-oxidation process. In more detail, the evidence suggests that, in the competition between the protective effect of silicates and the pro-oxidative effects typical of impurities, such as iron [42–45], the former outbalances the latter here.

However, the focus of the present study is the actual generation of microplastics.

Figure 2, therefore, shows the size distribution (in terms of weight fractions) of the generated fragments (including non-microplastic particles, >5 mm as discussed in the Introduction) for the PP and the NPP unweathered, unphoto-oxidized samples. As a first observation, particles having a size larger than 5 mm should be observed, since they are not considered microplastics [12]. The interesting result is that there is a significant difference between the neat PP and the NPP, since the latter has a significantly higher value, therefore the amount of released microplastics is significantly lower, about 1 wt% in total. This suggests not only that the nanofiller particles are well embedded in the polymer matrix and are therefore not individually released, but also that the overall interaction between the polymer matrix and the nanofiller particles, probably due to the organic modifier, is so good that it effectively imparts a reduction in polymer matrix nanoparticle release.

As regards the photo-oxidized (48 h, 96 h) samples, Figure 3, this overall trend seems to be maintained. However, it can also be observed that the generation of microplastics increases (i.e., the generation of particles with size > 5 mm decreases), at longer times, by approx. 10% in the PP and 4% in the NPP samples, respectively, thus widening the gap already observed in the case of neat, unphoto-oxidized samples. This seems to suggest that the presence of the nanoclay enhances the resistance to embrittlement and, therefore, to fragmentation and microplastic release. Indeed, this is in complete agreement with the results coming from the mechanical characterization that were previously described.

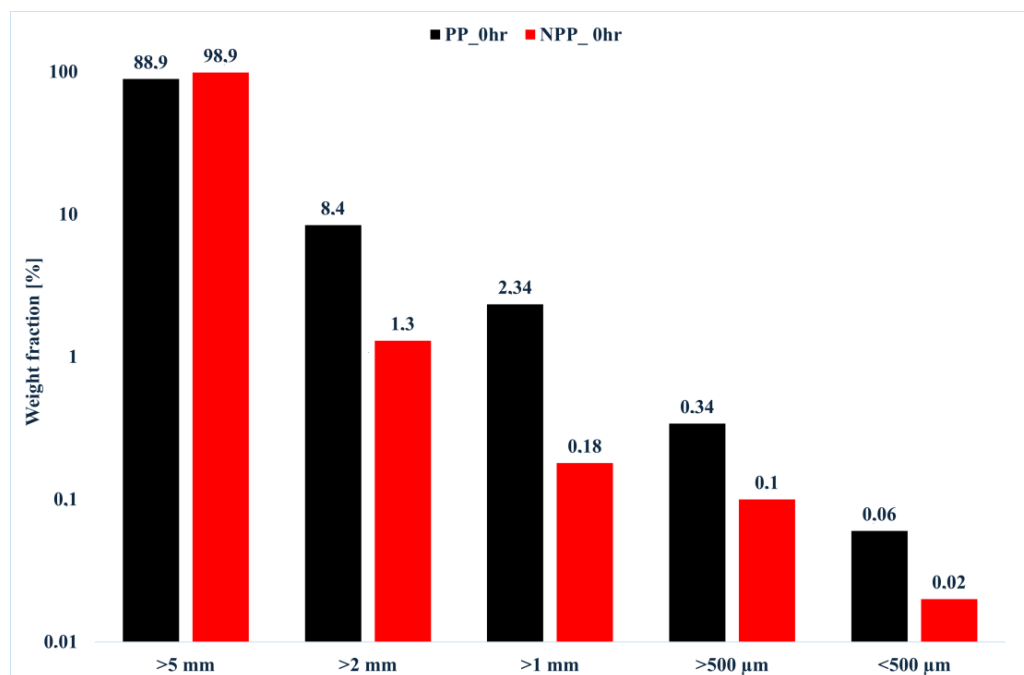


Figure 2. Size distribution of the generated fragments (non-microplastic particles > 5 mm) for the neat PP and the NPP unweathered, unphoto-oxidized samples.

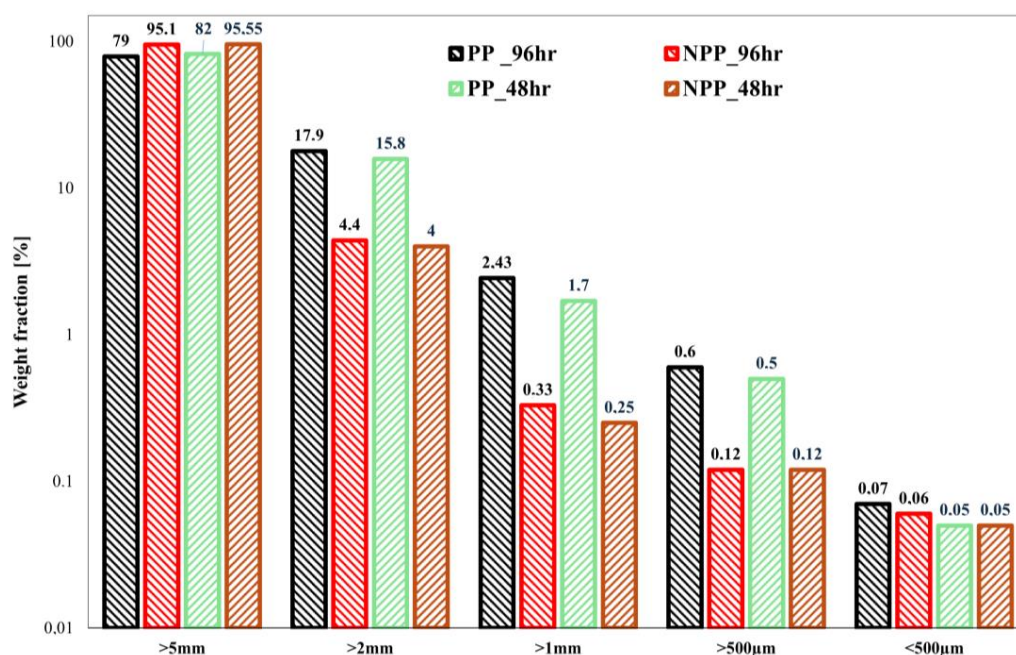


Figure 3. Size distribution of the generated fragments (non-microplastic particles > 5 mm) for the photo-oxidized (48 h, 96 h) PP and NPP samples.

At this point, further interpretation of these results is needed and proposed, as follows.

As briefly hinted previously, the nanofiller is likely to mitigate the embrittlement related to the photo-oxidation process because of the protective effect of silicates [42–45]. In more detail, this also suggests that the other possible negative effects due to a nanoclay filler as described in the cited studies (i.e., formation of catalytic acidic sites due to the decomposition of ammonium ions, and additional production of radicals from the oxidation of the modifier alkyl chain) do not significantly occur here, or at least occur to a lesser extent in comparison to the protective action from the silicates.

The above considerations were further proved and deepened by performing a spectroscopic analysis based on FT-IR.

Figure 4 shows the spectra of unirradiated PP and nanocomposite, as well as the nanoclay.

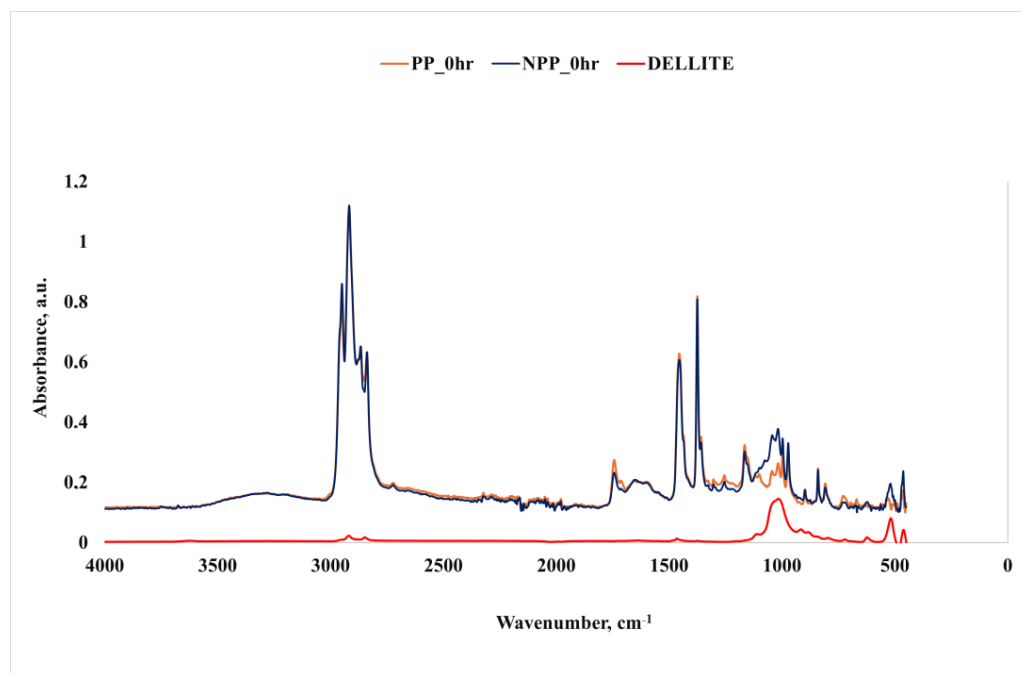


Figure 4. FTIR spectra of unirradiated PP, NPP and nanoclay samples.

With regard to the spectrum of the nanoclay, the following main peaks were observed: -OH stretching and hydration at approx. 3500 and 1650 cm^{-1} , and, in particular, the very low intensity of the peaks demonstrates the prevalently hydrophobic nature of the organically modified clay in comparison to a standard clay [46–48]; a high intensity peak around 1020 cm^{-1} related to Si-O stretching, in-plane; and two remarkable peaks at about 520 and 450 cm^{-1} , attributable to Si-O-Al deformation vibration and Si-O-Si bending, respectively [46,47,49]. Further peaks around 2920 and 2850 cm^{-1} are related to the CH_2 asymmetric and symmetric stretching mode, respectively [50–54], while those around 750 and 1450 can be attributed to the CH_2 rocking and scissoring mode, respectively, with the peak at 1460 attributable to the presence of an aromatic ring [50,51,53]. A schematic summary is provided in Table 4.

Table 4. FTIR peaks and related attributions.

| Peak [cm^{-1}] | Attribution |
|---------------------------|-------------------------------------|
| 3500 | -OH stretching |
| 2920 | CH_2 asymmetric stretching |
| 2850 | CH_2 symmetric stretching |
| 1650 | -OH hydration |
| 1450 | CH_2 scissoring |
| 1020 | Si-O stretching, in-plane |
| 750 | CH_2 rocking |
| 520 | Si-O-Al deformation |
| 450 | Si-O-Si bending |

Regarding the spectra of the polymer and the nanocomposite, it is easy to observe that the former is a typical PP spectrum, while the latter clearly presents the main bands of both the polymer and the nanoclay.

Figure 5, on the other hand, reports the FTIR spectra of the weathered samples. In this case, as expected, significant bands around 3500 cm^{-1} , due to hydroxyl groups, and $1680\text{--}1770\text{ cm}^{-1}$, due to carbonyl groups, appear, due to the photo-oxidation processes.

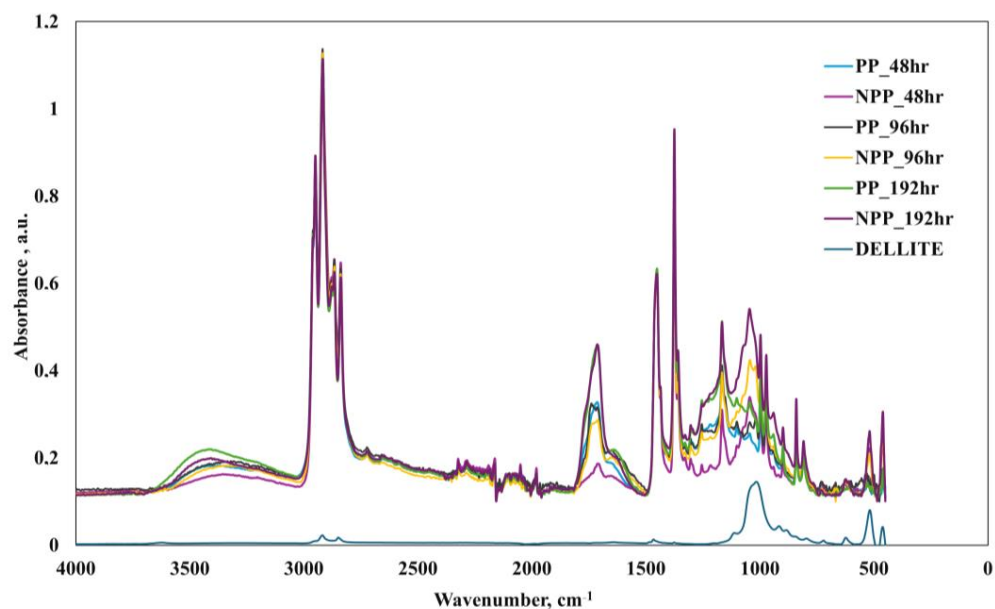


Figure 5. FTIR spectra of photo-oxidized PP, NPP and nanoclay samples.

A clearer observation can be made in Figure 6, highlighting the carbonyl region and the significantly smaller peak of NPP_48hr in comparison to PP_48hr. In more detail, peaks centered at approx. $1680\text{--}1710$, $1730\text{--}1740\text{ cm}^{-1}$, and $1770\text{--}1780\text{ cm}^{-1}$, attributable to, respectively, the formation of carboxylic acids, ketones, and esters and lactones due to photo-oxidation [42,55], should be observed. The nanocomposite samples show lower peaks at approx. 1710 and 1740 cm^{-1} , thus suggesting that the presence of the nanoclay helps in reducing the formation of photo-oxidation products, especially ketones and esters (resulting in a reduced carbonyl-related band) and therefore exerting a moderately protective effect. This is in complete agreement with the considerations made before, based on the results coming from mechanical tests and from the size distribution of the generated macro- and microplastics, thus providing further confirmation of the previously given discussions (which were based on the results from mechanical tests and actual microplastic generation). Nevertheless, the differences between the peaks of corresponding PP and NPP samples decrease upon increasing the exposure time; at significantly longer exposure times (i.e., 192 h), even the NPP eventually fails. Indeed, as discussed previously, the tensile and fragmentation tests were practically impossible to carry out due to the extreme brittleness of the PP, but also of the NPP samples. This is in substantial agreement with the reported FTIR peaks for PP and NPP after 192 h.

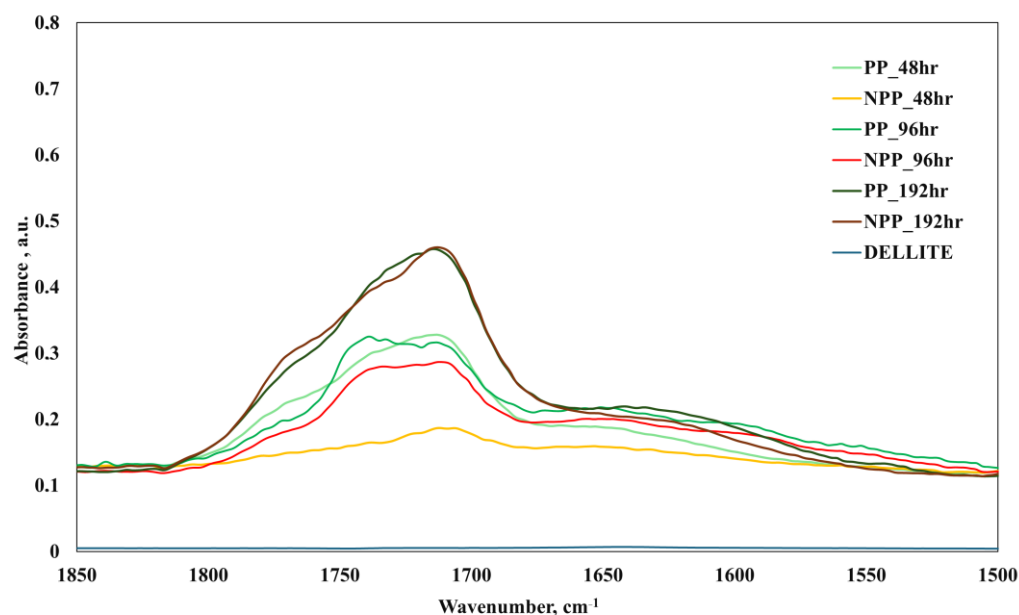


Figure 6. FTIR spectra of photo-oxidized (48 h, 96 h, 192 h) PP, nanocomposite and nanoclay samples.

In order to confirm that the observed benefit is not offset by inorganic nanoparticle release, we also carried out TGA measurements on pristine (unphoto-oxidized, unfragmented) PP and NPP, as well as unphoto-oxidized and fragmented NPP (FNPP), and photo-oxidized and fragmented NPP (PFNPP) and the nanoclay for comparison purposes. The residual mass (i.e., ash content) as % of initial mass of each sample is shown in the following Table 5 (thermograms reported in the Supplementary Materials, see Figure S2).

Table 5. Residual mass of samples after TGA.

| Sample | Residual Mass [%] |
|----------|-------------------|
| PP | 0.8 |
| NPP | 3.4 |
| Nanoclay | 64 |
| FNPP | 3 |
| PFNPP | 3 |

By comparing the ash content from the reference samples (PP, NPP, nanoclay) and the two nanocomposite samples, it can be observed that, while the nanoclay itself has a mass loss of about 35% (in agreement with other studies [56]) and the PP ash content is almost zero, thus explaining the residual mass of the pristine NPP, both the FNPP and the PFNPP have the same residual mass, and practically the same as NPP. This result allows for the conclusion that there was no significant nanoclay release.

However, it is appropriate to observe that this study contains some limitations which should be addressed in future studies, such as the presence of a single filler type and a single amount, the lack of a real-world aging environment, and therefore the use of a dry mechanical fragmentation method. Further studies should also be carried out regarding the actual balance (or imbalance) between the reduced microplastics formation on the one hand, and possibly increased environmental persistence on the other hand.

4. Conclusions

In this paper, PP/clay nanocomposite was subjected to photo-oxidation and mechanical fragmentation, thus simulating the two main generation mechanisms of micro- and

nanoplastics. A systematic characterization of the amount and size distribution of the obtained microplastics was then performed.

It was found that nanocomposite samples undergo less severe effects due to photo-oxidation, resulting in a lower decrease in the mechanical properties. This suggests that the nanofiller contributes to mitigating the embrittlement related to the photo-oxidation process, likely due to the protecting effect of silicate, which outbalances the pro-oxidative effects typical of impurities.

This was reflected in the results from the measurement of generated particle size distribution: nanocomposite samples generated more macroplastics (size > 5 mm) and therefore less micro- and nanoplastics. This result can be correlated to the previously reported observation that the nanoclay mitigates the embrittlement related to the photo-oxidation process. Further demonstration was achieved by FTIR analysis, showing that the presence of the nanoclay helps in slowing down the formation of photo-oxidation products in the typical carbonyl region. Further studies are, however, needed to address some limitations such as the use of a single filler type and single loading, as well as the lack of a real-world aging environment.

Supplementary Materials: The following supporting information can be downloaded at: <https://www.mdpi.com/article/10.3390/nano16030201/s1>, Figure S1: XRD diffractograms of pristine Dellite and NPP; Figure S2: TGA thermograms on pristine (unphotooxidized, unfragmented) PP and NPP, unphotooxidized and fragmented NPP (FNPP), photooxidized fragmented NPP (PFNPP) and nanoclay for comparison.;

Author Contributions: Conceptualization, F.P.L.M. and M.M.; methodology, F.P.L.M. and M.M.; validation, E.I., F.P.L.M., M.M. and L.B.; formal analysis, F.P.L.M., M.M., E.I. and L.B.; investigation, E.I. and L.B.; writing—original draft preparation, M.M. and F.P.L.M.; writing—review and editing, M.M. and F.P.L.M.; visualization, E.I., M.M. and L.B.; supervision, F.P.L.M. All authors have read and agreed to the published version of the manuscript.

Funding: This paper is based on work partly supported by “Progetti Industriali INSTM” (National Interuniversity Consortium of Materials Science and Technology: INSTM, Italy) and partly supported by the Sicilian MicroNanotech Research and Innovation Center “Samothrace” project (Italian Ministry of University and Research: MUR, PNRR-M4C2, ECS_00000022).

Data Availability Statement: Data can be made available from the corresponding author(s) under reasonable request.

Acknowledgments: Thanks are due to Bartolomeo Megna for the support in performing the TGA tests.

Conflicts of Interest: The authors declare that they have no known competing financial interests or personal relationships that could have appeared to influence the work reported in this paper. The funders had no role in study design, data collection and analysis, the decision to publish, or preparation of the manuscript, which reflects the opinions of the authors.

References

1. Monkul, M.M.; Özhan, H.O. Microplastic contamination in soils: A review from geotechnical engineering view. *Polymers* **2021**, *13*, 4129. [[CrossRef](#)]
2. Jambeck, J.R.; Geyer, R.; Wilcox, C.; Siegler, T.R.; Perryman, M.; Andrady, A.; Narayan, R.; Law, K.L. Plastic waste inputs from land into the ocean. *Science* **2015**, *347*, 768–771. [[CrossRef](#)]
3. Abdelkader, N.; Ismail, S.B.; Zakhama-Sraieb, R. Macro-, meso- and microplastic debris in three sandy beaches of north-eastern Tunisian coasts. *Reg. Stud. Mar. Sci.* **2023**, *67*, 103229. [[CrossRef](#)]
4. Rezania, S.; Park, J.; Din, M.F.M.; Taib, S.M.; Talaiekhosani, A.; Yadav, K.K.; Kamyab, H. Microplastics pollution in different aquatic environments and biota: A review of recent studies. *Mar. Pollut. Bull.* **2018**, *133*, 191–208. [[CrossRef](#)] [[PubMed](#)]

5. Weber, C.J.; Hahn, J.; Opp, C. Spatial connections between microplastics and heavy metal pollution within floodplain soils. *Appl. Sci.* **2022**, *12*, 595. [[CrossRef](#)]
6. Nguyen, L.H.; Nguyen, B.S.; Lee, D.T.; Alomar, T.S.; Al Masoud, N.; Ghotekar, S.; Oza, R.; Raizada, P.; Singh, P.; Nguyen, V.H. A concept for Biotechnological minimizing of emerging plastic, micro and nano-plastics pollutants from the environment: A review. *Environ. Res.* **2023**, *216*, 114342. [[CrossRef](#)]
7. Singh, S.; Kumar, V.; Kapoor, D.; Bhardwaj, S.; Dhanjal, D.S.; Pawar, A.; Ramamurthy, P.; Singh, J. Fate and occurrence of micro and nano-plastic pollution in industrial wastewater. In *Biodegradation and Detoxification of Micropollutants in Industrial Wastewater*; Haq, I., Kalamdhad, A.S., Shah, M.P., Eds.; Elsevier: Amsterdam, The Netherlands, 2022; pp. 27–38.
8. Bhattacharya, P.A. Review on the impacts of microplastic beads used in cosmetics. *Acta Biomed. Sci.* **2016**, *3*, 47–52.
9. Issac, M.N.; Kandasubramanian, B. Effect of microplastics in water and aquatic systems. *Environ. Sci. Pollut. Res.* **2021**, *28*, 19544–19562. [[CrossRef](#)] [[PubMed](#)]
10. Vighi, M.; Bayo, J.; Fernández-Piñas, F.; Gago, J.; Gómez, M.; Hernández-Borges, J.; Rosal, R. Micro and nano-plastics in the environment: Research priorities for the near future. *Rev. Environ. Contam. Toxicol.* **2021**, *257*, 163–218.
11. Kiran, B.R.; Kopperi, H.; Venkata Mohan, S. Micro/nano-plastics occurrence, identification, risk analysis and mitigation: Challenges and perspectives. *Rev. Environ. Sci. Biotech.* **2022**, *21*, 169–203. [[CrossRef](#)] [[PubMed](#)]
12. Morreale, M.; La Mantia, F.P. Current Concerns about Microplastics and Nanoplastics: A Brief Overview. *Polymers* **2024**, *16*, 1525. [[CrossRef](#)]
13. Webb, H.K.; Arnott, J.; Crawford, R.J.; Ivanova, E.P. Plastic degradation and its environmental implications with special reference to poly (ethylene terephthalate). *Polymers* **2013**, *5*, 1–18. [[CrossRef](#)]
14. Musa, I.O.; Auta, H.S.; Ilyasu, U.S.; Aransiola, S.A.; Makun, H.A.; Adabara, N.U.; Abioye, O.P.; Aziz, A.; Jayanthi, B.; Maddela, N.R. Micro-and Nanoplastics in Environment: Degradation, Detection, and Ecological Impact. *Int. J. Environ. Res.* **2024**, *18*, 1. [[CrossRef](#)]
15. Stephens, B.; Azimi, P.; El Orch, Z.; Ramos, T. Ultrafine particle emissions from desktop 3D printers. *Atmos. Environ.* **2013**, *79*, 334–339. [[CrossRef](#)]
16. Koelmans, A.A.; Mohamed Nor, N.H.; Hermesen, E. Microplastics in freshwater and drinking water: Critical review and assessment of data quality. *Water Res.* **2019**, *155*, 410–422. [[CrossRef](#)] [[PubMed](#)]
17. Lambert, S.; Wagner, M. Characterisation of nanoplastics during the degradation of polystyrene. *Chemosphere* **2016**, *145*, 265–268. [[CrossRef](#)]
18. Sharma, S.; Chatterjee, S. Microplastic pollution, a threat to marine ecosystem and human health: A short review. *Environ. Sci. Pollut. Res.* **2017**, *24*, 21530–21547. [[CrossRef](#)]
19. Bank, M.S. *Microplastic in the Environment: Pattern and Process*; Springer Nature: Cham, Switzerland, 2022.
20. Auta, S.H.; Abioye, O.P.; Aransiola, S.A.; Bala, J.D.; Chukwuemeka, V.I.; Hassan, A.; Aziz, A.; Fauziah, S.H. Enhanced microbial degradation of PET and PS microplastics under natural conditions in mangrove environment. *J. Environ. Manag.* **2022**, *304*, 114273. [[CrossRef](#)]
21. Pignattelli, S.; Broccoli, A.; Piccardo, M.; Terlizzi, A.; Renzi, M. Effects of polyethylene terephthalate (PET) microplastics and acid rain on physiology and growth of *Lepidium sativum*. *Environ. Pollut.* **2021**, *282*, 116997. [[CrossRef](#)]
22. Arthur, C.; Baker, J.E.; Bamford, H.A. *Proceedings of the International Research Workshop on the Occurrence, Effects, and Fate of Microplastic Marine Debris*; University of Washington Tacoma: Tacoma, WA, USA, 2009.
23. Fu, W.; Min, J.; Jiang, W.; Li, Y.; Zhang, W. Separation. Characterization and Identification of Microplastics and Nanoplastics in the Environment. *Sci. Total Environ.* **2020**, *721*, 137561. [[CrossRef](#)]
24. Caputo, F.; Vogel, R.; Savage, J.; Vella, G.; Law, A.; Della Camera, G.; Hannon, G.; Peacock, B.; Mehn, D.; Ponti, J. Measuring Particle Size Distribution and Mass Concentration of Nanoplastics and Microplastics: Addressing Some Analytical Challenges in the Sub-Micron Size Range. *J. Colloid Interface Sci.* **2021**, *588*, 401–417. [[CrossRef](#)]
25. Van Cauwenberghe, L.; Devriese, L.; Galgani, F.; Robbins, J.; Janssen, C.R. Microplastics in Sediments: A Review of Techniques, Occurrence and Effects. *Mar. Environ. Res.* **2015**, *111*, 5–17. [[CrossRef](#)]
26. Alexy, P.; Anklam, E.; Emans, T.; Furfari, A.; Galgani, F.; Hanke, G.; Koelmans, A.; Pant, R.; Saveyn, H.; Sokull Kluettgen, B. Managing the Analytical Challenges Related to Micro- and Nanoplastics in the Environment and Food: Filling the Knowledge Gaps. *Food Addit. Contam. Part A* **2020**, *37*, 1–10. [[CrossRef](#)]
27. Vethaak, A.D.; Legler, J. Microplastics and Human Health. *Science* **2021**, *371*, 672–674. [[CrossRef](#)]
28. Ivleva, N.P. Chemical Analysis of Microplastics and Nanoplastics: Challenges, Advanced Methods, and Perspectives. *Chem. Rev.* **2021**, *121*, 11886–11936. [[CrossRef](#)] [[PubMed](#)]
29. Vianello, A.; Boldrin, A.; Guerriero, P.; Moschino, V.; Rella, R.; Sturaro, A.; Da Ros, L. Microplastic Particles in Sediments of Lagoon of Venice, Italy: First Observations on Occurrence, Spatial Patterns and Identification. *Estuar. Coast. Shelf Sci.* **2013**, *130*, 54–61. [[CrossRef](#)]

30. Qiu, Q.; Peng, J.; Yu, X.; Chen, F.; Wang, J.; Dong, F. Occurrence of Microplastics in the Coastal Marine Environment: First Observation on Sediment of China. *Mar. Pollut. Bull.* **2015**, *98*, 274–280. [[CrossRef](#)]
31. Kalogerakis, N.; Karkanorachaki, K.; Kalogerakis, G.C.; Triantafyllidi, E.I.; Gotsis, A.D.; Partsinevelos, P.; Fava, F. Microplastics Generation: Onset of Fragmentation of Polyethylene Films in Marine Environment Mesocosms. *Front. Mar. Sci.* **2017**, *4*, 84. [[CrossRef](#)]
32. Julienne, F.; Delorme, N.; Lagarde, F. From Macroplastics to Microplastics: Role of Water in the Fragmentation of Polyethylene. *Chemosphere* **2019**, *236*, 124409. [[CrossRef](#)]
33. Julienne, F.; Lagarde, F.; Delorme, N. Influence of the Crystalline Structure on the Fragmentation of Weathered Polyolefines. *Polym. Degrad. Stab.* **2019**, *170*, 109012. [[CrossRef](#)]
34. Dimassi, S.N.; Hahladakis, J.N.; Yahia, M.N.D.; Ahmad, M.I.; Sayadi, S.; Al-Ghouti, M.A. Degradation-Fragmentation of Marine Plastic Waste and Their Environmental Implications: A Critical Review. *Arab. J. Chem.* **2022**, *15*, 104262. [[CrossRef](#)]
35. Wei, X.F.; Nilsson, F.; Yin, H.; Hedenqvist, M.S. Microplastics Originating from Polymer Blends: An Emerging Threat? *Environ. Sci. Technol.* **2021**, *55*, 4190–4193. [[CrossRef](#)]
36. La Mantia, F.P.; Baiamonte, M.; Titone, V.; Botta, L.; Morreale, M. Role of compatibilization on the disintegration of polymer blends and their release of micro- and nanoplastics. *Macromol. Mat. Eng.* **2026**. *submitted for publication*.
37. Alipour, N.; Strömberg, E.; Enebro, J.; Hedenqvist, M.S. Release of micro-and nanoparticles from a polypropylene/clay nanocomposite, a methodology for controlled degradation and evaluation. *J. Clean. Prod.* **2021**, *319*, 128761. [[CrossRef](#)]
38. Bossa, N.; Sipe, J.M.; Berger, W.; Scott, K.; Kennedy, A.; Thomas, T.; Wiesner, M.R. Quantifying mechanical abrasion of MWCNT nanocomposites used in 3D printing: Influence of CNT content on abrasion products and rate of microplastic production. *Environ. Sci. Technol.* **2021**, *55*, 10332–10342. [[CrossRef](#)]
39. Sahle-Demessie, E.; Han, C.; Varughese, E.; Acrey, B.; Zepp, R. Fragmentation and release of pristine and functionalized carbon nanotubes from epoxy-nanocomposites during accelerated weathering. *Environ. Sci. Nano* **2023**, *10*, 1812–1827. [[CrossRef](#)]
40. Sipe, J.M.; Berger, W.; Bossa, N.; Chernick, M.; Scott, K.C.; Kennedy, A.; Wiesner, M.R. Quantifying mechanical abrasion of AgNP nanocomposites: Influence of AgNP content on abrasion products and rate of microplastic production. *Environ. Sci. Nano* **2024**, *11*, 2968–2977. [[CrossRef](#)]
41. La Mantia, F.P.; Baiamonte, M.; Titone, V.; Botta, L.; Morreale, M. Fragmentation of polypropylene/polyethylene terephthalate (PP/PET) polymer blends and generation of micro and nanoplastics: Effect of compatibilization. *Mat. Lett.* **2025**, *395*, 138695. [[CrossRef](#)]
42. Morreale, M.; Dintcheva, N.T.; La Mantia, F.P. The role of filler type in the photo-oxidation behaviour of micro-and nano-filled polypropylene. *Polym. Int.* **2011**, *60*, 1107–1116. [[CrossRef](#)]
43. Morlat-Therias, S.; Fanton, E.; Gardette, J.L.; Dintcheva, N.T.; La Mantia, F.P.; Malatesta, V. Photochemical stabilization of linear low-density polyethylene/clay nanocomposites: Towards durable nanocomposites. *Polym. Degrad. Stab.* **2008**, *93*, 1776–1780. [[CrossRef](#)]
44. Mailhot, B.; Morlat, S.; Gardette, J.L.; Boucard, S.; Duchet, J.; Gerard, J.F. Photodegradation of polypropylene nanocomposites. *Polym. Degrad. Stab.* **2003**, *82*, 163–167. [[CrossRef](#)]
45. Leroux, F.; Medder, L.; Mailhot, B.; Morlat-Therias, S.; Gardette, J.L. Characterization and photooxidative behaviour of nanocomposites formed with polystyrene and LDHs organo-modified by monomer surfactant. *Polymer* **2005**, *46*, 3571–3578. [[CrossRef](#)]
46. Antosik, A.K.; Mozelewska, K. Influence of Nanoclay on the Thermo-Mechanical Properties of Silicone Pressure-Sensitive Adhesives. *Materials* **2022**, *15*, 7460. [[CrossRef](#)]
47. Yu, C.; Ke, Y.; Hu, X.; Zhao, Y.; Deng, Q.; Lu, S. Effect of bifunctional montmorillonite on the thermal and tribological properties of polystyrene/montmorillonite nanocomposite. *Polymers* **2019**, *11*, 834. [[CrossRef](#)]
48. Morreale, M.; Dintcheva, N.T.; La Mantia, F.P. Accelerated weathering of PP based nanocomposites: Effect of the presence of maleic anhydride grafted polypropylene. *Express Polym. Lett.* **2013**, *7*, 703–715. [[CrossRef](#)]
49. Angaji, M.T.; Rafiee, R.; Hemmati, M.; Abdollahi, M.; Razavi Aghjeh, M.K. Parametric studies on the grafting of poly (methylmethacrylate) onto organophilic montmorillonite using silylated clay platelets. *J. Macromol. Sci. B* **2014**, *53*, 957–974. [[CrossRef](#)]
50. Wójcik-Bania, M.; Matusik, J. The Effect of Surfactant-Modified Montmorillonite on the Cross-Linking Efficiency of Polysiloxanes. *Materials* **2021**, *14*, 2623. [[CrossRef](#)]
51. Silverstein, R.M.; Webster, F.X.; Kiemle, D.J.; Bryce, D.L. *Spectrometric Identification of Organic Compounds*, 8th ed.; Wiley: Hoboken, NJ, USA, 2014.
52. Zhu, J.; He, H.; Zhu, L.; Wen, X.; Deng, F. Characterization of organic phases in the interlayer of montmorillonite using FTIR and ¹³C NMR. *J. Colloid Interface Sci.* **2005**, *286*, 239–244. [[CrossRef](#)]
53. Zope, I.S.; Dasari, A.; Yu, Z.-Z. Influence of Polymer-Clay Interfacial Interactions on the Ignition Time of Polymer/Clay Nanocomposites. *Materials* **2017**, *10*, 935. [[CrossRef](#)]
54. Slaný, M.; Jankovič, L.; Madejová, J. Structural characterization of organo-montmorillonites prepared from a series of primaryalkylamines salts: Mid-IR and near-IR study. *Appl. Clay Sci.* **2019**, *176*, 11–20. [[CrossRef](#)]

55. Zhou, Y.; Li, B.; Zhang, P. Fourier transform infrared (FT-IR) imaging coupled with principal component analysis (PCA) for the study of photooxidation of polypropylene. *Appl. Spectrosc.* **2012**, *66*, 566–573. [[CrossRef](#)] [[PubMed](#)]
56. Bertini, F.; Canetti, M.; Leone, G.; Tritto, I. Thermal behavior and pyrolysis products of modified organo-layered silicates as intermediates for in situ polymerization. *J. Anal. Appl. Pyrolysis* **2009**, *86*, 74–81. [[CrossRef](#)]

Disclaimer/Publisher’s Note: The statements, opinions and data contained in all publications are solely those of the individual author(s) and contributor(s) and not of MDPI and/or the editor(s). MDPI and/or the editor(s) disclaim responsibility for any injury to people or property resulting from any ideas, methods, instructions or products referred to in the content.